Modeling Compressible Viscous Fluid-Solid Interaction Using a Nitsche-Based Finite Element Method

Hamideh Hassanpour Guilvaiee[1], Florian Toth[2], Manfred Kaltenbacher[3]

[1] *Institute of Mechanics and Mechatronics, TU Wien, Vienna, Austria, Email: hamideh.hassanpour@tuwien.ac.at*

[2] *Institute of Mechanics and Mechatronics, TU Wien, Vienna, Austria, Email: florian.toth@tuwien.ac.at*

[2] *Institute of Fundamentals and Theory in Electrical Engineering (IGTE), TU Graz, Graz, Austria*

Email: manfred.kaltenbacher@tugraz.at

Introduction

Micro-electro-mechanical systems (MEMS) technology has a wide range of applications in constructing micro transducers and microsensors. They are used in medical applications, e.g., ultrasound imaging [1], and non-destructive structure testing [2]. In this work, we model a MEMS ultrasound transducer using the finite element method. We first discuss formulations needed to model the ultrasound transducer then, we demonstrate the finite element formulation followed by our 3D application example.

Governing Equations

In modeling MEMS ultrasound transducers, we model the solid field with piezoelectric effect, the near field acoustic with thermoviscous effects, and the far-field acoustic. The viscous compressible near field flow is defined by the conservation of mass, momentum, and energy. We use the perturbation ansatz (in the conservation of mass, momentum, and energy) for the pressure p, the density ρ, the temperature T and the velocity $\boldsymbol{v}$ to separate the acoustic field from the fluid field

$$\bar{p} = p_0 + p(\boldsymbol{x},t)\,, \qquad \bar{\rho} = \rho_0 + \rho(\boldsymbol{x},t)\,,$$
$$\bar{T} = T_0 + T(\boldsymbol{x},t)\,, \qquad \bar{\boldsymbol{v}}(\boldsymbol{x}) = \boldsymbol{v}_0 + \boldsymbol{v}(\boldsymbol{x},t)\,,$$

where the bar $\bar{(.)}$ and $(.)_0$ denote the total and the temporally constant background quantities, respectively. The rest are the perturbation quantities, which are assumed to be small. Further assumption such as zero mean flow ($\boldsymbol{v}_0 = 0$) and zero source terms in the conservation of mass, momentum, and energy is considered. We insert these perturbations into the conservation relations and ignore the non-linear terms. To remove the destiny degree of freedom the linearized equation of state (for general fluid) is considered

$$\rho = \rho_0\left(\beta_\mathrm{T} p - \alpha_\mathrm{p} T\right)\,,$$
$$\beta_\mathrm{T} = \frac{1}{\rho_0}\left(\frac{\partial \rho_\mathrm{a}}{\partial p}\right)_{T_0} = \frac{1}{\rho_0}\frac{\gamma}{c^2}\,,$$
$$\alpha_\mathrm{p} = -\frac{1}{\rho_0}\left(\frac{\partial \rho_\mathrm{a}}{\partial T}\right)_{p_0} = \frac{1}{c}\sqrt{\frac{c_\mathrm{p}(\gamma-1)}{T_0}}\,, \tag{1}$$

where β_T and α_p are the coefficient of compressibility and isobaric coefficient of thermal expansion, respectively. In these relations, γ, c_p and c denotes the adiabatic exponent, specific heat capacity at constant pressure and the speed of sound ($c = \sqrt{K/\rho_0}$ is computed from the adiabatic bulk modulus K), respectively. By applying Fourier's law, the heat flux $\boldsymbol{q}$ is related to the temperature gradient (∇T) by thermal conductivity κ

$$\boldsymbol{q} = \kappa \nabla T\,. \tag{2}$$

The viscous stress tensor $\boldsymbol{\sigma}_\mathrm{v}$ in conservation of momentum for an isotropic Newtonian fluid is

$$\boldsymbol{\sigma}_\mathrm{v} = -p\boldsymbol{I} + \mu\big(\boldsymbol{\nabla}\boldsymbol{v} + (\boldsymbol{\nabla}\boldsymbol{v})^T\big) + (\lambda - \frac{2}{3}\boldsymbol{u})(\boldsymbol{\nabla}\cdot\boldsymbol{v})\boldsymbol{I}\,, \tag{3}$$

where $\boldsymbol{I}$, μ and λ are the unity tensor, the fluid shear and bulk viscosity, respectively. Considering above assumptions, the final set of conservations describing the linearized compressible viscous flow are

$$\rho_0\frac{\partial \boldsymbol{v}}{\partial t} - \nabla\cdot\boldsymbol{\sigma}_\mathrm{v} = \boldsymbol{0} \quad \text{in } \Omega_\mathrm{v}\,, \tag{4}$$

$$\frac{\gamma}{c^2}\frac{\partial p}{\partial t} - \frac{\rho_0}{c}\sqrt{\frac{c_\mathrm{p}(\gamma-1)}{T_0}}\frac{\partial T}{\partial t} + \nabla\cdot(\rho_0\boldsymbol{v}) = 0 \quad \text{in } \Omega_\mathrm{v}\,, \tag{5}$$

$$\rho_0 c_\mathrm{p}\frac{\partial T}{\partial t} + \nabla\cdot\boldsymbol{q} - \frac{\partial p}{\partial t} = 0 \quad \text{in } \Omega_\mathrm{v}\,. \tag{6}$$

In the far field acoustic (Ω_a), neglecting the viscous and thermal effects are usually appropriate. Therefore we will not solve the conservation of energy and its effect on the pressure and velocity. In addition, we assume $\mu = \lambda = 0$ which allows to remove the velocity and obtaining the acoustic wave equation for the acoustic pressure p_a

$$\frac{\partial^2 p_\mathrm{a}}{\partial t^2} - c^2\nabla\cdot\nabla p_\mathrm{a} = 0 \quad \text{in } \Omega_\mathrm{a}\,. \tag{7}$$

In solid domain we satisfy the conservation of the momentum

$$\rho_\mathrm{s}\frac{\partial^2 \boldsymbol{u}}{\partial t^2} - \boldsymbol{\nabla}\cdot\boldsymbol{\sigma}_\mathrm{s} = \boldsymbol{0} \quad \text{in } \Omega_\mathrm{s}\,, \tag{8}$$

where ρ_s is the solid density, $\boldsymbol{u}$ is the displacement and $\boldsymbol{\sigma}_\mathrm{s}$ is the mechanical stress tensor. For the more details on the solid assumptions and piezoelectric formulation see our previous work [3].

Finally, we will apply the coupling and boundary conditions. The displacement and velocity are considered zero on the wall boundaries in solid and thermoviscous acoustics, respectively. On the symmetry boundaries, their

normal component will be zero. In addition, the thermoviscous acoustics harmonic temperature variations on the wall and the normal acceleration in the acoustic partial differential equation (PDE) are zero. This corresponds to homogeneous Neumann boundary conditions.

The coupling conditions between (piezoelectric) solid and thermoviscous acoustics at solid-thermoviscous acoustics interfaces (Γ_{sv}) are dynamic and kinematic conditions, requiring continuity of traction and continuity of velocity

$$\boldsymbol{\sigma}_{\mathrm{s}} \cdot \boldsymbol{n} = \boldsymbol{\sigma}_{\mathrm{v}} \cdot \boldsymbol{n} \quad \text{and} \quad \frac{\partial \boldsymbol{u}}{\partial t} = \boldsymbol{v} \quad \text{on } \Gamma_{\mathrm{vs}}\,, \tag{9}$$

respectively. The outer normal vector $\boldsymbol{n}$ is the outer normal vector of the thermoviscous acoustics and the inverse outer normal of the solid domain ($\boldsymbol{n} = \boldsymbol{n}_{\mathrm{v}} = -\boldsymbol{n}_{\mathrm{s}}$). The coupling conditions between either thermoviscous acoustics or solid regions with acoustic formulations similarly enforces the dynamic and kinematic conditions

$$\boldsymbol{\sigma}_i \cdot \boldsymbol{n} = -p_{\mathrm{a}}\boldsymbol{n}, \quad \text{and} \quad \frac{\partial \boldsymbol{v}_i}{\partial t} \cdot \boldsymbol{n} = -\frac{1}{\rho_0}\nabla p_{\mathrm{a}} \cdot \boldsymbol{n} \quad \text{on } \Gamma_{\mathrm{ai}}\,, \tag{10}$$

where $i = \mathrm{v}, \mathrm{s}$ defining viscous or solid domains. The outer normal $\boldsymbol{n}$ is defined as $\boldsymbol{n} = \boldsymbol{n}_i = -\boldsymbol{n}_{\mathrm{a}}$.

Finite Element Formulations

In the finite element formulation, the weak form is obtained by multiplying the test functions (donated by $()'$) to the governing PDEs and integrating over the computational domain. Introducing p' and T' as the test functions of pressure and temperature, respectively, the weak forms of conservation mass and energy in the thermoviscous acoustic region are

$$\int_{\Omega} \frac{\gamma}{c^2} p' \frac{\partial p}{\partial t}\,\mathrm{d}\Omega - \int_{\Omega} \frac{\rho_0}{c}\sqrt{\frac{c_{\mathrm{p}}(\gamma-1)}{T_0}}\, p' \frac{\partial T}{\partial t}\,\mathrm{d}\Omega + \int_{\Omega} \rho_0 p' \nabla \cdot \boldsymbol{v}_{\mathrm{a}}\,\mathrm{d}\Omega = 0 \tag{11}$$

$$\int_{\Omega} \rho_0 c_{\mathrm{p}} T' \frac{\partial T}{\partial t}\,\mathrm{d}\Omega + \int_{\Omega} \kappa \nabla T' \cdot \nabla T\,\mathrm{d}\Omega - \int_{\Omega} T' \frac{\partial p}{\partial t}\,\mathrm{d}\Omega + \int_{\Gamma} T' \boldsymbol{q} \cdot \boldsymbol{n}\,\mathrm{d}\Gamma = 0 \tag{12}$$

The thermoviscous acoustics-solid and thermoviscous acoustics-acoustics coupling conditions are applied on thermoviscous acoustics conservation of momentum. In the thermoviscous acoustics-solid coupling, the conditions are applied by using Nitsche method. In this method the traction continuity is directly applied to surface integrals. In contrast, the velocity continuity is applied by adding the jump term defined as

$$\beta \frac{p_{\mathrm{e}}^2}{h_{\mathrm{e}}} \int_{\Gamma_{\mathrm{vs}}} (\boldsymbol{u}' - \boldsymbol{v}') \cdot (\frac{\partial \boldsymbol{u}}{\partial t} - \boldsymbol{v})\,\mathrm{d}\Gamma = \boldsymbol{0}\,, \tag{13}$$

to the conservation of momentum in thermoviscous acoustics and solid regions. The jump term contains the element order $p_{\mathrm{e}} = \max(p_{\mathrm{s}}, p_{\mathrm{f}})$ to account various polynomial orders, where, p_{s} and p_{v} are the order of basic functions for solid and thermoviscous domains, respectively. Furthermore, we add $1/h_{\mathrm{e}}$ to the penalty term, where $h_{\mathrm{e}} = \min(h_{\mathrm{v}}, h_{\mathrm{s}})$ i.e. the smallest element length of thermoviscous acoustics or solid elements on the interface. This guarantees that the resulting system is positive definite [4]. The high value of the penalty factor results in a high condition number of the arising system matrix, however, its low value will not satisfy the continuity of the velocities. Therefore, we compare the penalty terms to the other terms (in solid and thermoviscous conversation of momentum) to obtain following scaling for the penalty factor

$$\beta_{\mathrm{scaling}} = (\frac{E}{h_{\mathrm{s}}\omega} + \frac{\mu}{h_{\mathrm{f}}})\frac{h_{\mathrm{e}}}{p_{\mathrm{e}}^2}\,, \tag{14}$$

where E, ω are the Young's modulus and the angular velocity, respectively. This scaling term ensures that the bi-linear forms including the penalty factor are in the order of magnitude of the other bi-linear terms. To enforce the continuity of velocity at the interface, we propose to scale the penalty term by including the user-defined numerical penalty factor β_{numeric} as

$$\beta = \beta_{\mathrm{scaling}}\beta_{\mathrm{numeric}}\,. \tag{15}$$

Therefore, the conservation of momentum for the viscous fluid (including solid coupling) reads as

$$\int_{\Omega_{\mathrm{f}}} \rho_0 \boldsymbol{v}' \cdot \frac{\partial \boldsymbol{v}}{\partial t}\,\mathrm{d}\Omega + \int_{\Omega_{\mathrm{f}}} \boldsymbol{\nabla}\boldsymbol{v}' : \boldsymbol{\sigma}_{\mathrm{v}}\,\mathrm{d}\Omega + \int_{\Gamma_{\mathrm{vs}}} \boldsymbol{v}' \cdot \boldsymbol{\sigma}_{\mathrm{s}} \cdot \boldsymbol{n}\,\mathrm{d}\Gamma - \beta \frac{p_{\mathrm{e}}^2}{h_{\mathrm{e}}} \int_{\Gamma_{\mathrm{vs}}} \boldsymbol{v}' \cdot (\frac{\partial \boldsymbol{u}}{\partial t} - \boldsymbol{v})\,\mathrm{d}\Gamma = \boldsymbol{0}\,. \tag{16}$$

To couple the acoustic wave equation to the thermoviscous acoustics formulation, we directly apply the dynamic and the kinematic transmission conditions according to equation (10) by inserting into the weak form of thermoviscous acoustic balance of momentum (16) and acoustic PDE. Moreover, the acoustic-solid continuity of normal acceleration is applied on the acoustic wave equation [5]. This leads to the final version of acoustic PDE that includes thermoviscous acoustic and solid couplings

$$\int_{\Omega_{\mathrm{a}}} \frac{1}{c_0^2}\psi \frac{\partial^2 p_{\mathrm{a}}}{\partial t^2}\,\mathrm{d}\Omega + \int_{\Omega_{\mathrm{a}}} \nabla\psi \cdot \nabla p_{\mathrm{a}}\,\mathrm{d}\Omega + \int_{\Gamma_{\mathrm{va}}} \rho_0 \psi\, \frac{\partial v}{\partial t} \cdot \boldsymbol{n}\,\mathrm{d}\Gamma - \int_{\Gamma_{\mathrm{sa}}} \rho_0 \psi\, \frac{\partial^2 u}{\partial t^2} \cdot \boldsymbol{n}\,\mathrm{d}\Gamma = 0\,, \tag{17}$$

where ψ is the test function of the acoustic pressure. The final version of conservation of momentum for the thermoviscous acoustics containing solid and acoustic coupling resulted from (16) is

$$\int_{\Omega_{\mathrm{v}}} \rho_0 \boldsymbol{v}' \cdot \frac{\partial \boldsymbol{v}}{\partial t}\,\mathrm{d}\Omega + \int_{\Omega_{\mathrm{v}}} \boldsymbol{\nabla}\boldsymbol{v}' : \boldsymbol{\sigma}_{\mathrm{v}}\,\mathrm{d}\Omega + \int_{\Gamma_{\mathrm{va}}} \boldsymbol{v}' \cdot p_{\mathrm{a}}\boldsymbol{n}\,\mathrm{d}\Gamma + \int_{\Gamma_{\mathrm{vs}}} \boldsymbol{v}' \cdot \boldsymbol{\sigma}_{\mathrm{s}} \cdot \boldsymbol{n}\,\mathrm{d}\Gamma - \beta \frac{p_{\mathrm{e}}^2}{h_{\mathrm{e}}} \int_{\Gamma_{\mathrm{vs}}} \boldsymbol{v}' \cdot (\frac{\partial \boldsymbol{u}}{\partial t} - \boldsymbol{v})\,\mathrm{d}\Gamma = \boldsymbol{0}\,. \tag{18}$$

The final version of solid conservation of momentum including piezoelectric effects, thermoviscous acoustic and acoustic coupling are

$$\int_{\Omega_s \cup \Omega_p} \boldsymbol{u}' \cdot \rho_s \frac{\partial^2 \boldsymbol{u}}{\partial t^2} \, \mathrm{d}\Omega + \int_{\Omega_s \cup \Omega_p} \boldsymbol{\mathcal{B}}(\boldsymbol{u}') : \boldsymbol{C} : \boldsymbol{\mathcal{B}}(\boldsymbol{u}) \, \mathrm{d}\Omega + \int_{\Omega_p} \boldsymbol{\mathcal{B}}(\boldsymbol{u}') : \boldsymbol{e} \cdot \boldsymbol{\nabla}\phi \, \mathrm{d}\Omega + \int_{\Gamma_{as}} \boldsymbol{u}' \cdot \boldsymbol{n} \, p_a \, \mathrm{d}\Gamma - \int_{\Gamma_{vs}} \boldsymbol{u}' \cdot \boldsymbol{\sigma}_s \cdot \boldsymbol{n} \, \mathrm{d}\Gamma + \beta \frac{p_e^2}{h_e} \int_{\Gamma_{vs}} \boldsymbol{u}' \cdot (\frac{\partial \boldsymbol{u}}{\partial t} - \boldsymbol{v}) \, \mathrm{d}\Gamma = \boldsymbol{0}\,, \quad (19)$$

$$- \int_{\Omega_p} \boldsymbol{\nabla}\phi' \cdot \boldsymbol{e} : \boldsymbol{\mathcal{B}}(\boldsymbol{u}) \, \mathrm{d}\Omega + \int_{\Omega_p} \boldsymbol{\nabla}\phi' \cdot \boldsymbol{\epsilon} \cdot \boldsymbol{\nabla}\phi \, \mathrm{d}\Omega = 0, \quad (20)$$

where, $\boldsymbol{u}'$ and ϕ' are the test functions for displacement and electric scalar potential ϕ, $\boldsymbol{s} = \boldsymbol{\mathcal{B}}(\boldsymbol{u})$ is the solid strain tensor, C and $\boldsymbol{e}$ denote material stiffness tensor and piezoelectric coupling tensor. The surface terms illustrate the traction continuity between solid-thermoviscous acoustics on surface Γ_{vs} and solid-acoustic on surface Γ_{as}.

The final set of formulations modeling solid with piezoelectric effects, thermoviscous acoustic and acoustic PDE are illustrated in equations (11), (12), (18), (19) and (20). These described formulations are implemented in the open-source finite element framework openCFS [6].

Example Problem

We model a 3D MEMS ultrasound transducer as an application example using described modeling strategies. Figure 1 shows the piezoelectric region in this transducer. The top electrodes are separated from each other (dark gray) and cover 50 % of the surface area to avoid electrical shorts and reduce the power consumption. The solid region consists of two layers silicon and PZT-5H. The transducer close to the slit is simulated by the thermoviscous acoustic to capture the viscous and thermal effects. The acoustic PDE simulates the other acoustic regions. Below the actuator is the acoustic back volume with a volume of 0.52 mm^3. The further domain dimensions and material properties are provided in Table 1 and Table 2, respectively. Figure 2 demonstrates the regions modeled in this example including thermoviscous acoustic, acoustic and solid (PZT and silicon) regions.

Results

We apply the potential of 1 V to excite the transducer. Furthermore, the absorbing boundary condition is considered around the acoustic region to simulate the far-field conditions. Figure 3(a) shows that the solid deformation (displacement magnitude) at the tip of the solid region is higher than the other parts. The displacement (y-axis) at the tip of solid are plotted in Fig. 3(b) over the frequency. The pick of the frequency at 80 kHz depicts the first resonance frequency with the displacement of ∼49 µm.

The vibration of the solid region leads to the acoustic pressure variations in thermoviscous acoustic and acoustic regions. Figure 4(a) depicts the acoustic pressure field at the first resonance frequency. This figure shows the higher pressure at the back volume and the pressure distribution in the far-field. At the point sensor (Fig. 4(a)), with the distance of 3 cm from the source, the sound pressure level (SPL) is plotted over the frequency in Fig. 4(b). The maximum SPL of transducer reaches ∼120 dB at the frequency of ∼80 kHz.

How large the thermoviscous region should be to capture the viscous and thermal effects may pose a question. To study this question we have proposed and studied this example for various thermoviscous radii r_{thv} = 20, 40, 60, 80, 100 µm. We consider the larger thermoviscous region (r_{thv} = 100µm) has the most precise results. Therefore, we consider this radios as the reference solution and compared the relative error norm as $\frac{||p_i - p_{100}||}{||p_{100}||} \times 100, i = 20, 40, 60, 80$. Figure 5 shows the average relative error at the frequencies of 1, 70, 79, 80 and 80.25 kHz over the radios. By increasing the ra-

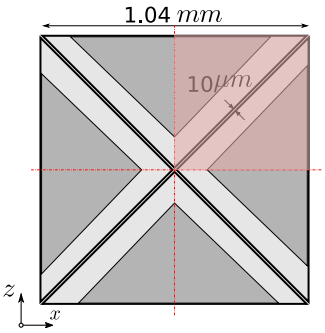

Figure 1: Piezoelectric actuator. Dark gray regions show the top electrode. Due to symmetry, the signed red region is simulated.

Property	Value (µm)
Transducer	
Silicon thickness	10
Piezo thickness	2
Transducer length	1040
Thermoviscous Region	
slit thickness	10
Radios r_{thv}	60
Acoustic Region	
Radios r_{acou}	12000

Table 1: Geometry dimensions

Property	Silicon
Density ρ in kg/m^3	2329
Young's modulus E in Pa	$1.12 \cdot 10^{11}$
Poisson's ratio ν_E	0.28

Property	Fluid (Air)
Density ρ_v in kg/m^3	1.225
Bulk modulus K in Pa	$1.4271 \cdot 10^5$
Dynamic viscosity μ in Pas	$1.829 \cdot 10^{-5}$
Bulk viscosity λ in Pas	$1.22 \cdot 10^{-5}$
Adiabatic exponent γ	1.406
Specific heat capacity c_p in J/K	975.3
Thermal conductivity κ in W/(mK)	$25.18 \cdot 10^{-3}$

Property		PZT-5H
Density ρ in kg/m^3		7500
Stiffness tensor $\mathbf{C}$ in N/m^2	$C_{11} = C_{22}$	$1.2720 \cdot 10^{11}$
	C_{33}	$1.1744 \cdot 10^{11}$
	$C_{12} = C_{21}$	$8.0212 \cdot 10^{10}$
	$C_{13} = C_{31}$	$8.4670 \cdot 10^{10}$
	$C_{23} = C_{32}$	$8.4670 \cdot 10^{10}$
	$C_{44} = C_{55}$	$2.2989 \cdot 10^{10}$
	C_{66}	$2.3496 \cdot 10^{10}$
Permittivity $\boldsymbol{\epsilon}$ in F/m	$\epsilon_{11} = \epsilon_{22}$	$2.771 \cdot 10^{-8}$
	ϵ_{33}	$3.010 \cdot 10^{-8}$
Piezoelectric coupling tensor $\mathbf{e}$ in As/m^2	$e_{31} = e_{32}$	-6.6228
	e_{33}	23.240
	$e_{24} = e_{15}$	17.034

Table 2: Material parameters [3].

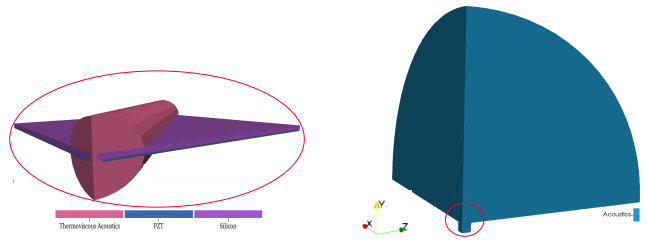

(a) Thermoviscous acoustic and solid regions

(b) Acoustic region with the back volume of 0.52 mm^3

Figure 2: Ultrasound transducer regions

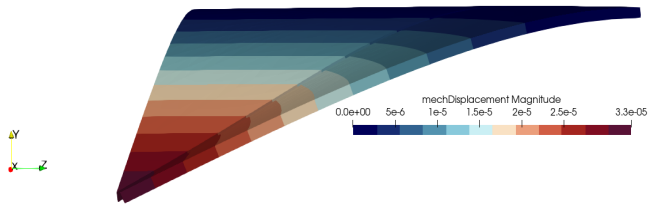

(a) Solid deformation at f = 80 kHz

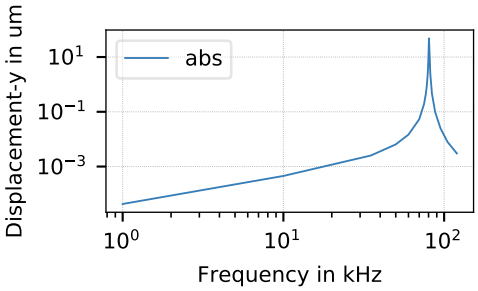

(b) Displacement at the tip of the cantilever

Figure 3: Piezoelectric displacement deformations

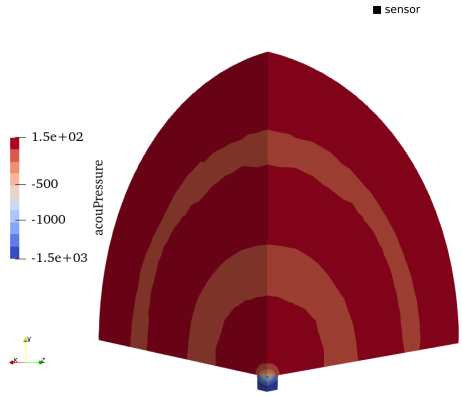

(a) Far-field acoustic pressure field at f = 80 kHz

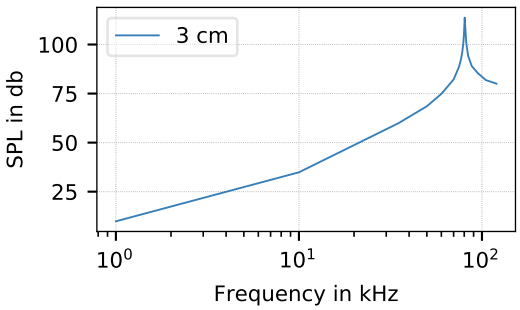

(b) Sound pressure level at distance = 3 cm

Figure 4: Acoustic pressure and sound pressure level

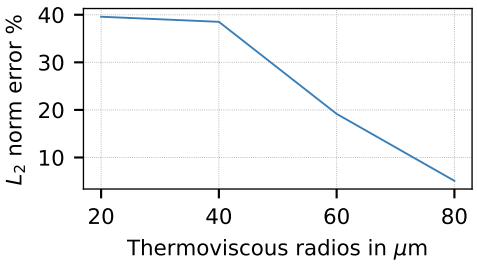

Figure 5: Pressure L_2 norm error

dios, the error decreases, and at the radios of 80 µm the system produces the error of 5 %. Not that the computational time of 100 µm is 8.5 times the computational time needed for the 80 µm. We consider this radios as an acceptable value for doing further study on the system.

Conclusion

In the presented MEMS ultrasound transducer, we model the thermoviscous effects in the acoustic pressure propagation close to the solid structures. The thermoviscous effects are captured with the linearized Navier-Stokes formulations and then is coupled to piezoelectric and acoustic domains to model the transducer. The proposed model created the sound pressure level of the 120 dB at the frequency of ∼ 80 kHz. We further studied the effect of various thermoviscous regions on the acoustic far-field pressure. The results showed the relative error between radii of 80 and 100 µm is 5 %. Considering the high computational effort needed for the larger thermoviscous regions, we choose 80 µm as the optimized dimension.

Acknowledgments

This work was partly funded by the Austrian Research Promotion Agency (FFG) within the program line "Bridge" (project number 868033).

References

[1] Ira O. Wygant, Xuefeng Zhuang, David T. Yeh, Ömer Oralkan, A. Sanli Ergun, Mustafa Karaman, and Butrus T. Khuri-Yakub. Integration of 2D CMUT arrays with front-end electronics for volumetric ultrasound imaging. *IEEE Transactions on Ultrasonics, Ferroelectrics, and Frequency Control*, 55(2):327–341, 2008.

[2] Irving J. Oppenheim, Akash Jain, and David W. Greve. MEMS ultrasonic transducers for the testing of solids. *IEEE Transactions on Ultrasonics, Ferroelectrics, and Frequency Control*, 50(3):305–311, 2003.

[3] Florian Toth, Hamideh Hassanpour Guilvaiee, and Georg Jank. Acoustics on small scales: Modelling viscous effects in MEMS devices. *Elektrotechnik und Informationstechnik*, 2021.

[4] A. Fritz, S. Hüeber, and B. I. Wohlmuth. A comparison of mortar and Nitsche techniques for linear elasticity. *Calcolo*, 41(3):115–137, 2004.

[5] Manfred Kaltenbacher. *Numerical Simulation of Mechatronic Sensors and Actuators*. Springer Berlin Heidelberg, Berlin, Heidelberg, 2015.

[6] Manfred Kaltenbacher, Florian Toth, and Hamideh Hassanpour. openCFS, www.opencfs.org.